Next Sustainability 1 (2023) 100008

Contents lists available at ScienceDirect

Next Sustainability

journal homepage: www.sciencedirect.com/journal/next-sustainability

Research article

Room-temperature direct regeneration of spent $LiFePO_4$ cathode using the external short circuit strategy

Chenglei Li [a,1], Hao Du [a,1], Yuqiong Kang [a], Yun Zhao [a,*], Yao Tian [a], John Wozny [b], Jian Lu [a], Tao Li [b], Naser Tavajohi [c], Ming Huang [d], Bo Lan [d], Feiyu Kang [a], Baohua Li [a,*]

[a] Institute of Materials Research, Tsinghua Shenzhen International Graduate School, Tsinghua University, Shenzhen 518055, China
[b] Department of Chemistry and Biochemistry, Northern Illinois University, DeKalb, IL 60115, USA
[c] Department of Chemistry, Umeå University, Umeå 90187, Sweden
[d] Department of Mechanical Engineering, Imperial College London, London SW7 2AZ, United Kingdom

ARTICLE INFO

Keywords:
Spent lithium-ion batteries
Direct cathode regeneration
External short-circuit
Lithium supplementation

ABSTRACT

Lithium iron phosphate batteries (LFP), widely used as power sources, are forecasted to reach the terawatt-hour scale, inevitably leading to battery waste and expediating the urgency for effective recycling processes for LFP. The modern recycling methodologies based on material recovery face significant economic, environmental, and energy consumption challenges. This research attempts to resolve these challenges by providing direct cathode regeneration based on the principles of an external short-circuit to replenish lithium lost in the spent cathode with lithiated materials (LiC_6, Li metal). Given that most active lithium loss in the cathode is caused by the growth of the solid electrolyte interphase rather than structural damage, restoring the lost lithium can revitalize a spent cathode battery's electrochemical performance to a near-original state. The lithium loss in LFP cathodes ranging from 20% to 80% was renewed by supplementing lithium. Relithiation of 10Ah commercial LFP spent cathode showed revitalized electrochemical performance. Compared to the modern recycling methods, direct cathode regeneration improves the economic benefits of recycling by 33%, decreases energy consumption by 48%, and reduces carbon emissions by 62%. Direct cathode regeneration provides a scaffold for the next generation of recycling methods to improve recycling efficiency while reducing their environmental footprint.

Introduction

Lithium-ion batteries (LIBs) are crucial in electronics, electric vehicles, and large-scale energy storage due to their high energy density and long service life [1]. Humanities' reliance on technology and LIBs as the preferred power source has increased demand for LIBs worldwide, with the global shipping volume of LIBs is projected to reach 3.2 TWh by 2030 [2,3]. However, LIBs have a limited lifespan (between 5 and 10 years for advanced batteries), and the rapid growth of the battery market is projected to generate millions to tens of millions of spent LIBs annually [4]. Recycling spent LIBs has become increasingly crucial regarding resource consumption, environmental pollution, and energy security [5].

Lithium iron phosphate ($LiFePO_4$) battery (LFP) is an olivine-type material and one of the three mainstream cathode materials for LIBs, which includes layered transition metal oxide [6,7], spinel-like [8], and other olivine-type materials [9–11]. The highest demand for LFP cathodes is in LIB batteries. LIBs accounted for approximately 60% of the battery market share in 2022 and are projected to exceed the terawatt-hour scale by 2030. Therefore, a practical battery recycling strategy based on these chemistries has become increasingly relevant. Unfortunately, traditional pyrometallurgy (pyro), hydrometallurgy (hydro), and direct material regeneration methods suffer from low-profit margins, high consumption, emissions, complex processing, and low recycling efficiency. These methods generally require the battery to be discharged due to safety risks. Followed by pretreatment, physical and chemical processes adding dozens of additional steps to the recycling workflow. These factors currently hinder recycling manufacturers from creating a more sustainable LIBs future [12–17].

Pyrometallurgy and hydrometallurgy methods can extract essential elements from the battery materials. Still, these methods may not be the best options for recycling lithium, as the binder and conductive agents in

* Corresponding authors.
E-mail addresses: yzhao.zjut@hotmail.com, yun.zhao22@imperial.ac.uk (Y. Zhao), libh@mail.sz.tsinghua.edu.cn (B. Li).
[1] These authors contributed to this work equally.

https://doi.org/10.1016/j.nxsust.2023.100008
Received 30 August 2023; Received in revised form 23 September 2023; Accepted 11 October 2023
Available online 17 October 2023
2949-8236/© 2023 The Authors. Published by Elsevier Ltd. This is an open access article under the CC BY-NC-ND license (http://creativecommons.org/licenses/by-nc-nd/4.0/).

the cathode materials cannot be entirely removed. Achieving acceptable purity levels from the crushed battery remains complicated and energy intensive. After the LIBs are pulverized, they can only be converted into a $LiFePO_4$ and a carbon materials mixture with a heat treatment under inert gas [18–27]. Direct material regeneration is more straightforward and can recycle spent LIBs at the material level. Such strategies depend on the spent LIBs materials and components with high to mild reparability characteristics. However, recycling would be dramatically simplified if spent LIBs or their individual components could be effectively repaired or directly reused. This indirectly results in increased revenue, reduced consumption, improved workflow, and reduced cost of element or material re-manufacturing batteries.

Fortunately, LFP has a stable olivine crystal structure, and the strong interactions between the phosphorus and oxygen covalent bonds give the PO_4 tetrahedra excellent structural stability [28,29]. Damage to the crystal structure of the LFP cathode during long cycling is minimal. The main failure mechanisms are the loss of the active lithium source, electrolyte deterioration, and increased anode surface resistance [30, 31]. Therefore, directly replenishing lithium in the cathodes of spent LIBs can effectively recycle the cathode.

The proposed methodology offers a simple and efficient way to regenerate the LFP cathode material with lithium supplementation. It primarily uses lithiated materials in the form of lithiated graphite (LiC_6) and lithium metal. Using principles based on the external short-circuit, the lithium in the lithiated materials is supplemented into the spent LFP cathode through a self-discharge process, during which different lithium-deficient cathodes can be regenerated by controlling the lithium replenishment time. Various characterization measurements are then employed to validate that lithium can be supplemented into the spent LFP cathodes, revealing direct cathode regeneration. Microstructure characterization and electrochemical performance tests can be applied to assess regenerated commercial cathodes from spent batteries and help govern applicable processes. Compared to existing recycling strategies, direct cathode regeneration offers advantages to simplify the LIB recycling process and improve economic efficiency, providing a new approach for recycling cathode material through regeneration and reference values for the subsequent cathode regeneration research.

Results and discussion

Working mechanism of the external short-circuit regeneration for degraded $LiFePO_4$ cathode

Fig. 1a illustrates the process of lithium supplementation and the functional mechanism for external short-circuit regeneration. Previous studies have established that the main reason for capacity degradation in LFP batteries is due to the loss of active lithium sources and an increase in anode interfacial resistance [31,32]. The LFP cathodes serve as the source for the loss of active lithium, eventually leading to the degradation of the battery system and eventual battery failure. The anode is structurally damaged during the long cycling process, resulting in cracks at the solid electrolyte interface (SEI). During the regeneration of the SEI, the active lithium source is continuously consumed, leading to irreversible lithium loss from the battery.

In the crystal structure of $LiFePO_4$, Li^+ occupies the 4a site of the octahedral co-edge, and Fe^{2+} occupies the 4c site of the octahedral co-angle; lithium vacancy appears at the 4a site due to the loss of the active lithium source [33]. The presence of the three-dimensional P-O-Fe bonds in the crystal structure lattice does not readily undergo oxygen evolution, and it helps maintain the structure from distortion or collapse during long charge cycles [34]. The cathode crystal structure transforms between $LiFePO_4$ and $FePO_4$ phases during charge and discharge. During the charging process, the $LiFePO_4$ phase converts to $FePO_4$ as the lithium ions migrate out, forming the $FePO_4/LiFePO_4$ interface (Fig. S1). This interface moves toward the center of the particle, and the $LiFePO_4$ phase continues to shrink until the charging process ends or the number of migrating ions is no longer sufficient to maintain the limited charge current [35]. During the discharge process, the reverse process occurs, and the $FePO_4$ converts back to $LiFePO_4$, starting at the center of the particle. The $FePO_4/LiFePO_4$ interface continues to move toward the surface of the particle until all $FePO_4$ is converted back to $LiFePO_4$.

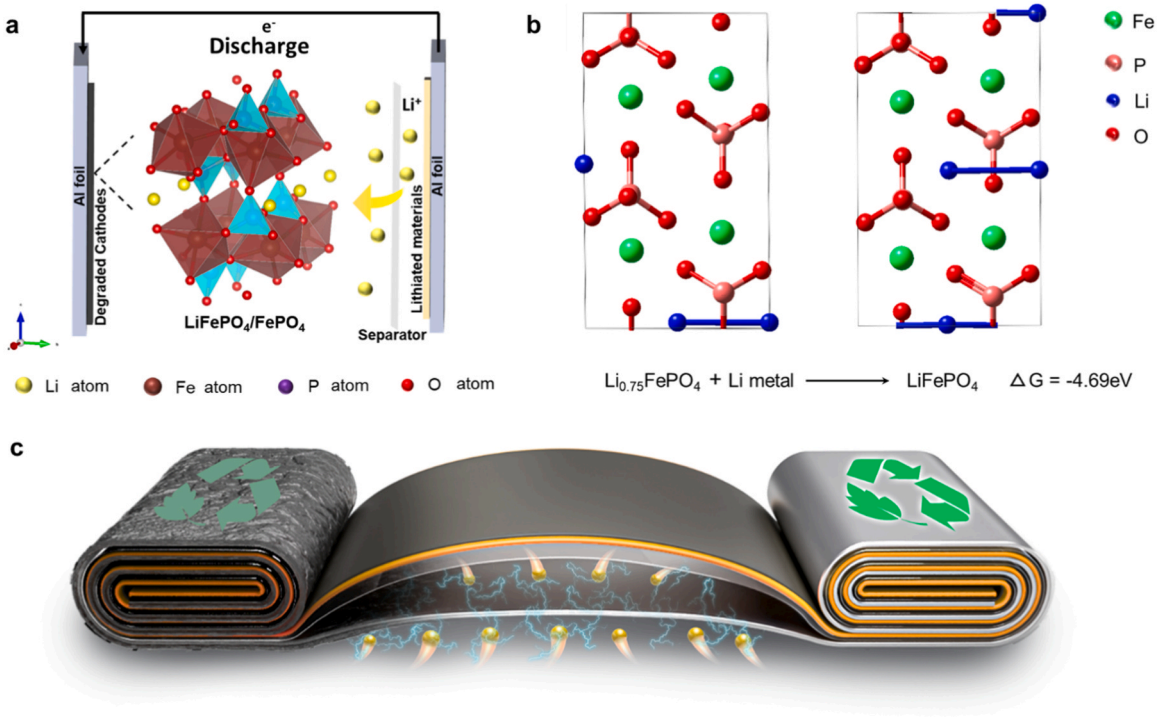


Fig. 1. Working mechanism of the external short-circuit regeneration. (a) The working mechanism of the external short-circuit regeneration at the crystal level. (b) The optimized Li-deficiency structures and reaction energies (Eadh) with Li atoms by VASP. (c) Schematic diagram of the spent battery regeneration.

The interactions between Li atoms and Li-deficiency cathodes ($Li_{0.75}FePO_4$) were further investigated by measuring the binding energy calculated by the first-principles Vienna Abinitio Simulation Package (VASP). As shown in Fig. 1b, the binding energy is −4.69 eV, indicating that the reaction can proceed spontaneously at room temperature, with the lithium ions replenished to the lithium-deficient 4a site by relying only on the potential of the internal material. After the reaction, the complete $LiFePO_4$ crystal structure is successfully restored.

Fig. 1c illustrates the schematic of the spent battery regeneration process. The external short-circuit regeneration method exploits how batteries discharge to form an external short-circuit structure that combines the lithiated materials with Li-deficiency $Li_{1-x}FePO_4$. The interaction between the partial $FePO_4$ phase (Li-deficiency $Li_{1-x}FePO_4$) and lithiated material creates a potential. Relying on the potential of the internal material as the driving force, the lithium ions in the lithiated materials can be supplemented into the lithium vacancies of the $Li_{1-x}FePO_4$ material. The partial $FePO_4$ phase converts to $LiFePO_4$, restoring the lithium in the crystal structure. No other energy was consumed during the regeneration process, the lithium vacancies are filled with lithium supplied by the lithiated material, and the regenerated cathodes restore the electrochemical performance essentially to their initial capacity.

Feasibility analysis of the external short-circuit regeneration strategy

A feasibility study was used to evaluate LFP cathode regeneration. Various $Li_{1-x}FePO_4$ cathodes were prepared for the degraded model compounds with different Li-deficiency states. The pristine LFP cathodes (P-LFP) and Li-deficient cathodes (D-LFP) can be achieved by controlling charge time at a current of 0.1 C. Four Li-deficiency cathodes were prepared with a charge time of 2, 4, 6, and 8 h and labeled D-LFP-2 h, D-LFP-4 h, D-LFP-6 h, and D-LFP-8 h, respectively. The ideal spent battery model would have x vary from 0 to 0.8 and mimic degraded LFP batteries in any charge state between 20% and 80%.

The presence of the $FePO_4$ phase in the D-LFP was identified in the XRD diffraction pattern results (Fig. 2a) and the enlarged patterns (Fig. 2b). These diffraction peaks at 18.10°, 20.60°, 23.72°, 25.72°, 30.44°, 30.98°, and 33.25° correspond to typical $FePO_4$ peaks (PDF #85–2384), corresponding to the (200), (101), (210), (111), (211), (020), and (301) planes, respectively [31]. The diffraction peak intensity of $FePO_4$ gradually increased with the loss of lithium. The galvanostatic charge test was carried out to obtain the initial charge capacity for each cathode sample (Fig. 2c). The initial charge capacity of P-LFP, D-LFP-2 h, D-LFP-4 h, D-LFP-6 h, and D-LFP-8 h was 167.1, 135.4, 101.5, 62.1, and 31.5 mAh g^{-1}, respectively. The results suggest the gradual decrease in initial capacity is related to the reduced active lithium in the LFP lattice.

Based on the amount of lithium loss in each Li-deficiency cathode sample, the external short-circuit relithiation method was performed by controlling the reaction time. The XRD pattern diffraction results exhibiting the typical diffraction peaks of $FePO_4$ in the D-LFP disappeared after relithiation with lithiated graphite (LiC_6) or lithium metal (Fig. 2d). The XRD diffraction pattern of regenerated LFP (R-LFP) contacted the LFP standard diffraction peak (PDF #83–2902). After external short-circuit relithiation, the initial charge capacity of all D-LFP samples was similar to the initial charge-discharge profiles of P-LFP (Fig. 2e), with the reversible capacity around 163.3 mAh g^{-1}, indicating that the external short-circuit relithiation method could intercalate the active Li^+ successfully into D-LFP lattice to compensate for the loss of the active lithium source.

It was observed that the open-circuit voltage (OCV) of the half cells could describe the degree of external short-circuit relithiation. The OCV was exposed to the oxidation state of Fe [36]. As shown in Fig. 2f, the OCV of the P-LFP half-cell was 3.26 V vs. Li^+/Li, but increased to 3.42 V for the D-LFP half-cell. The OCV of R-LFP was restored to 3.23 V after relithiation, which was similar to the P-LFP. This result suggests that active Li^+ could be intercalated successfully into the D-LFP lattice using the external short-circuit relithiation method, further demonstrating the feasibility of the external short-circuit regeneration strategy.

Structural evolution during the external short-circuit regeneration process

Generally, if the capacity of LIBs degrades below 80% of their initial capacity, the battery is considered retired or spent [37]. Therefore,

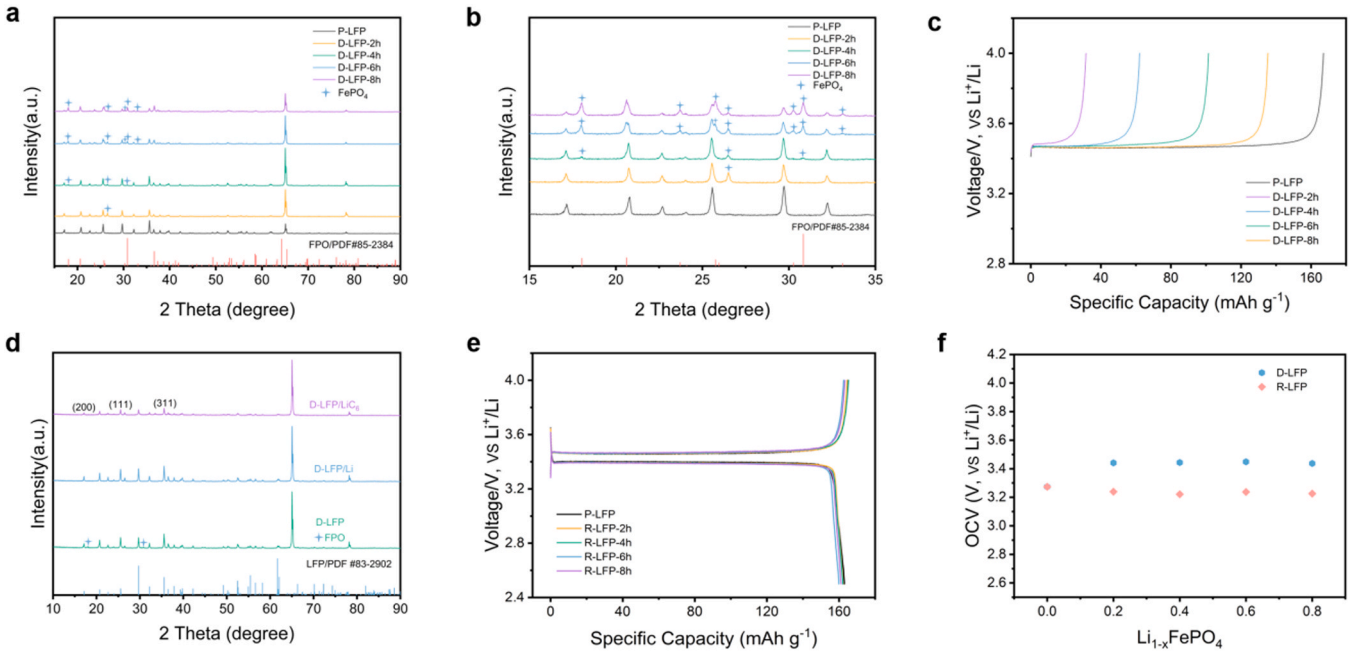


Fig. 2. Regeneration of Li-deficiency $Li_{1-x}FePO_4$ model compounds in different SOC using an external short-circuit regeneration strategy. (a) The XRD patterns of the LFP cathodes with various Li-deficiency states. (b) The enlarged XRD patterns of (a). (c) The initial charge capacity of Li-deficiency LFP cathodes at 0.1 C. (d) The XRD patterns of the regenerated LFP cathodes with different lithiated materials. (e) The initial charge-discharge capacity of regenerated LFP cathodes at 0.1 C. (f) The evolution of open-circuit voltage with the content of Li before and after lithium supplementation.

cathode sample D-LFP-4 h was considered a model spent battery with a lithium loss of about 40%. This cathode was used as a representative of electrochemically-aged cathode material for characterizing the crystal structure and oxidation state of Fe during the external short-circuit relithiation method. Accordingly, the regenerated material from D-LFP is labeled R-LFP unless otherwise indicated.

SEM was performed to characterize the effects of the external short-circuit relithiation process on the morphology of the cathode materials (Fig. 3a and S2). The high similarity in the particle size for D-LFP and R-LFP suggested that the external short-circuit relithiation process had a minimal impact on the cathodes' morphology. The surface of the cathodes after relithiation was smooth, with no apparent microcracks. The effects of the relithiation process on the internal microstructure of the D-LFP and R-LFP cathodes were performed by ion milling and CP characterizations. The ion-thinned cathode cross-sectional images are displayed in Fig. 3b and Fig. S3, and the CP longitudinal section images are shown in Fig. S4. There were no apparent defects in the internal structure of D-LFP or R-LFP, such as pores or microcracks, suggesting that the relithiation process has negligible effects on the morphology of a treated cathode's surface and interior.

The external short-circuit relithiation effects on the elemental valence of the cathode are further illustrated by the XPS spectra of the D-LFP and R-LFP in Fig. S5 and Fig. 3c. Fe 2p was divided into Fe $2p_{3/2}$ peaks and Fe $2p_{1/2}$ peaks at 710.6 and 724.4 eV in D-LFP due to the 2p spin-orbit coupling splitting. The Fe $2p_{3/2}$ peak was divided into 710.3 and 714.4 eV peaks, the oxidation states of Fe^{2+} and Fe^{3+}, respectively [38,39]. The Fe $2p_{1/2}$ peak was split into the Fe^{2+} peak at 724.3 eV and the Fe^{3+} peak at 729.6 eV [24,40]. The oxidation state of Fe^{3+} is attributed to the lithium deficiency. Based on the principle of electron conservation, Fe exists in the form of Fe^{2+} in the original $LiFePO_4$. During the charging process, due to the absence of Li^+ ions, material oxidation results in the formation of $FePO_4$ phase, leading to the presence of Fe^{3+}. In the XPS spectra of R-LFP, the oxidation state of Fe^{3+} was not measured, and the XPS spectrum is similar to P-LFP (Fig. S6). In-depth XPS was further used to investigate the valence state of Fe from the surface of the cathode (Fig. S7). For D-LFP, Fe $2p_{3/2}$ and Fe $2p_{1/2}$ peaks at 711.4 and 725.3 eV were attributed to the Fe^{3+}. The spectral peaks shifted to lower binding energy with increasing etching time, indicating the presence of Fe^{3+} on the D-LFP surface. For R-LFP, there is no oxidized state of Fe^{3+} present as Li is supplemented. The peaks at 710.2 and 723.8 eV attributed to Fe $_{2p3/2}$ and Fe $2_{p1/2}$ of Fe^{2+} did not change from the surface of the cathode, indicating the complete elimination of the $FePO_4$ phase after the relithiation process [38]. In addition, the P 2p, C 1 s, and O 1 s spectra were analyzed in detail (Fig. S8); the P 2p spectrum was divided into two peaks, 133.6 eV corresponding to P $2p_{3/2}$ and 134.4 eV corresponding to P $2p_{1/2}$ [41]. C 1 s were divided into four defined peaks centered at 284.8, 286.4, 288.3, and 290.6 eV, which correspond to C–C, C–O, C═O, and C–F bonds, respectively [42]. In the XPS spectrum of O 1 s, two peaks were observed at 530.28 and 533.7 eV, representing the Fe-O bond in the FeO_6 octahedron and the P-O bond in the PO_4 tetrahedron [15]. Therefore, the XPS results indicate that the external short-circuit relithiation process only affected Fe (i.e., none of the other elements) on the valence and content.

Considering the two-phase reaction during charge and discharge, the $LiFePO_4$ phase in the fully charged state theoretically completely converts to the $FePO_4$ phase, which in the fully discharged state converts to the $LiFePO_4$ phase [34]. To determine whether a complete two-phase reaction exists in R-LFP cathodes, in-situ XRD analysis was performed on a half cell with R-LFP as the cathode and lithium metal as the anode. The charge-discharge profile at the rate of 0.2 C and the phase change of the cathodes were monitored (Fig. 3d–f and Fig. S9). According to the in situ XRD patterns, the two-phase reaction was in the R-LFP cathodes during charging and discharging; the typical peaks of $LiFePO_4$ disappeared during the charging but appeared during the discharging. Combined with the HRTEM images, the coexistence of $LiFePO_4$ and $FePO_4$ phases is present during the charging plateau (Fig. 3g-m). After the half cell was charged to 4 V, the typical peak of the $LiFePO_4$ became invisible, indicating a complete phase transition from $LiFePO_4$ to $FePO_4$ (Fig. 3n-p). In-situ XRD patterns and HRTEM images further suggest that during discharge, Li^+ was inserted into the lattice of the cathodes to complete the phase conversion from $FePO_4$ to $LiFePO_4$ [43] (Fig. 3q-s). Moreover, TEM images and EDS spectra (Fig. S10) reveal that the carbon coating on the surface of R-LFP particles remained intact. The external short-circuit relithiation method of D-LFP cathode regeneration seems feasible.

The electrochemical performance of regenerated LFP cathodes

The electrochemical performance of the R-LFP cathodes was evaluated using half cells after lithium supplementation to validate the electrochemical activation of the R-LFP cathodes. The P-LFP cathode was used as the reference material. Fig. 4a and b exhibit the cyclic voltammetry (CV) curves of P-LFP and R-LFP samples at a sweep speed of 0.1 mV/s between 2.5 and 4.0 V. The first loop of P-LFP and R-LFP had a pair of redox peaks at 3.27/3.60 V attributed to the Fe^{2+}/Fe^{3+} redox peaks. Fe^{2+}/Fe^{3+} peaks of the subsequent CV loops appeared at the same position, indicating that the R-LFP had high electrochemical reversibility [44]. The initial charge capacity of R-LFP was 160.3 mAh g^{-1}at 0.1 C (1 C = 170 mAh g^{-1}) (Fig. 4c). The charge-discharge voltage plateau was ~3.4 V, consistent with the cyclic voltammetry data. P-LFP and R-LFP cathode rate capability was characterized by discharge capacities at varying currents. The discharge capacities displayed in Fig. 4d measured at 165.5 (0.1 C), 158.4 (0.2 C), 145.7 (0.5 C), 134.3 (1 C), and 119.2 mAh g^{-1} (2 C). When the charge-discharge current was restored to 0.5 C, the discharge capacity increased to 144.4 mAh g^{-1}. This signifies that R-LFP cathodes maintained their original structure and electrochemical stability at a high current. The long-term cycling stability was investigated for P-LFP, D-LFP, and R-LFP cathodes at 1 C (Fig. 4g). The Li-deficiency D-LFP cathode discharge capacity (mAh g^{-1}) rapidly degraded after 200 cycles. In comparison, the R-LFP showed a discharge capacity of 130.6 mAh g^{-1} after 100 cycles and 115.5 mAh g^{-1} after 500 cycles demonstrating good capacity retention (98.0% after 100 cycles and 88.4% after 500 cycles). The improvement in discharge capacity of the R-LFP cathode was attributed to lithium supplementation.

EIS was used to investigate the interfacial stability of P-LFP and R-LFP cathodes. It is widely acknowledged that the interface stability of batteries largely influences their electrochemical properties and performance. The influence of structure affects the cathode's electrochemical properties. P-LFP and R-LFP structural differences were characterized via the kinetics of lithium-ion diffusion and Nyquist plots (Fig. 4e). The $z' \sim \omega^{-1/2}$ fitted curves are shown in Fig. 4f [45]. The slope difference in the low-frequency region indicates variance in the lithium-ion diffusion kinetics [46]. According to the calculated equations (Eq. (1)), the lithium-ion diffusion coefficients of R-LFP and P-LFP were 1.74×10^{-14} cm^2 $s^{-1}$and 2.12×10^{-14} cm^2 s^{-1}, respectively, indicating the recovery of lithium-ion migration channels after relithiation:

$$D = \frac{R^2T^2}{2A^2n^4F^4C^2\sigma^2}, \quad (1)$$

where D is the diffusion coefficient of lithium-ion, R is the gas constant, T is the reaction temperature, A is the surface area of the electrode, n is the number of electrons transferred in the redox half-reaction, F is the Faraday constant, C is the concentration of lithium-ion in the $LiFePO_4$, and σ is the Warburg factor obtained from the equivalent circuit model in EIS (the slope of $z' \sim \omega^{-1/2}$).

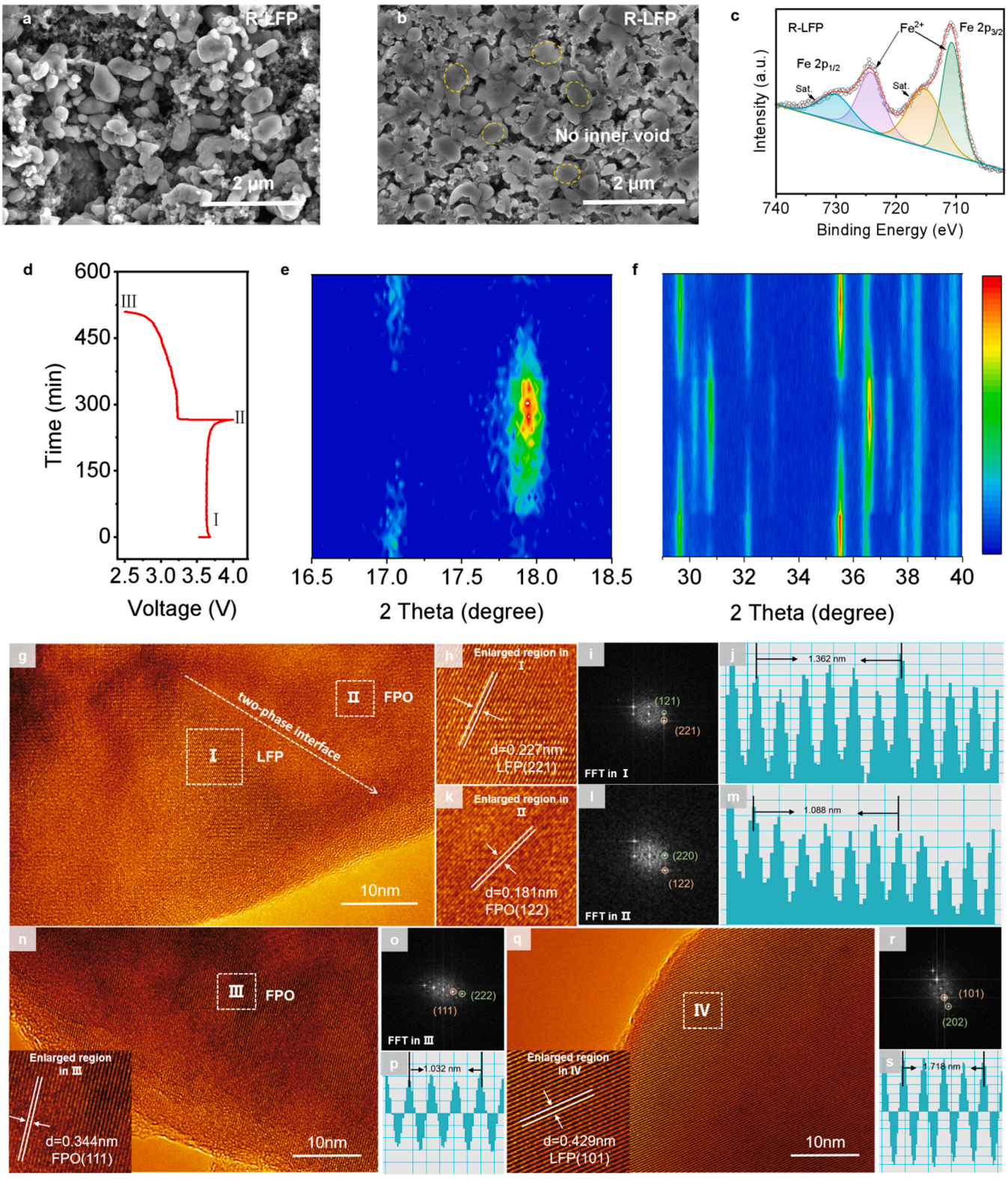


Fig. 3. Microstructure characterization of D-LFP and R-LFP. (a) SEM images of R-LFP. (b) SEM-CP images of R-LFP. (c) Fe 2p high-resolution XPS spectra of R-LFP. (d) The panel aligned with in situ XRD patterns of R-LFP during the initial charge and discharge at 0.2 C rate displays the half-cell voltage as a function of time. (e, f) correspond to the intensity contour maps of the evolution of the prominent characteristic diffraction peaks. (g–m) (n–p), and (q–s) correspond to the HRTEM images of the cathode particle at different states marked in I/II/III of (d).

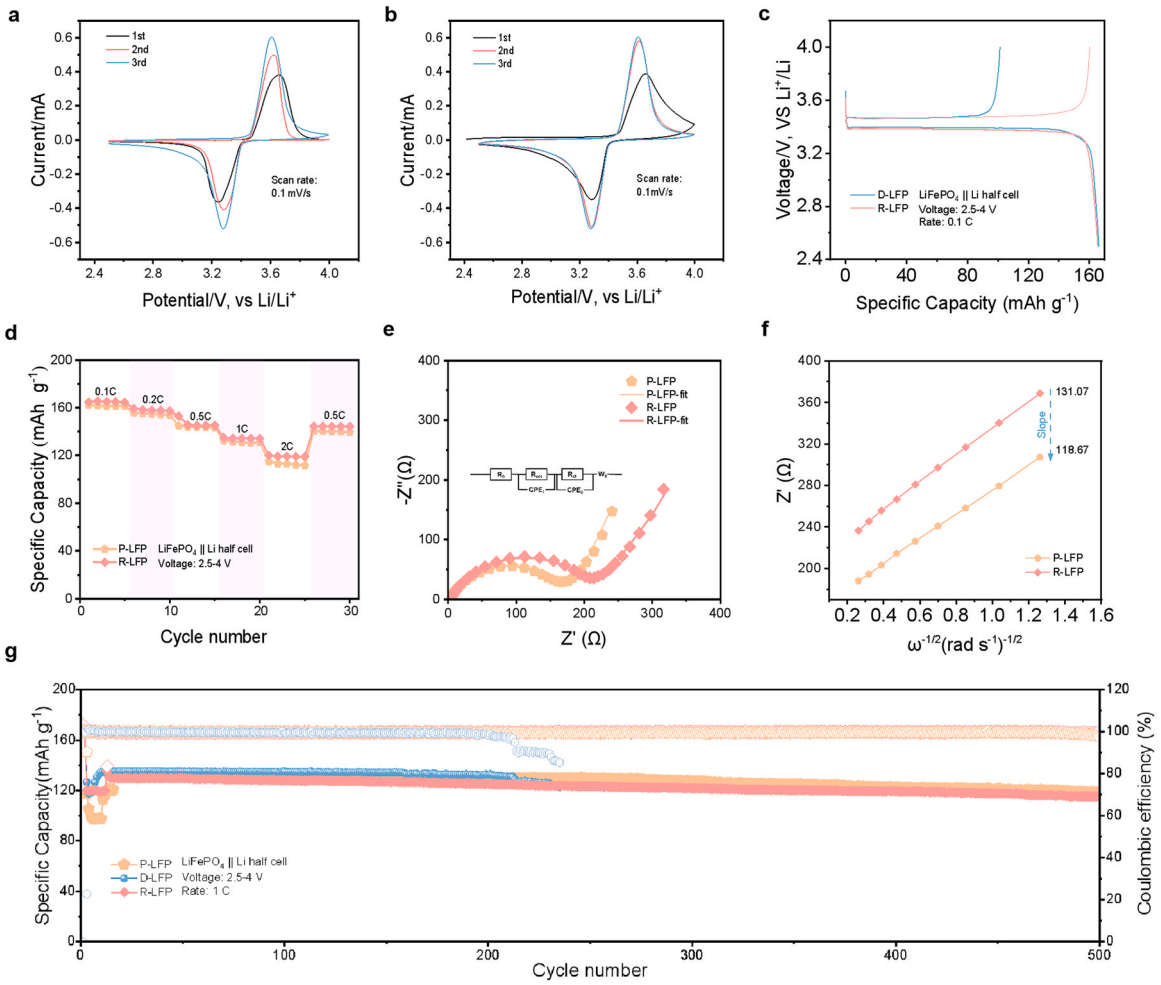


Fig. 4. The electrochemical performance of R-LFP. The cyclic voltammetry curves of (a) P-LFP and (b) R-LFP. (c) The initial charge and discharge profiles of D-LFP and R-LFP. (d) The rate performance test for P-LFP and R-LFP. (e) The electrochemical impedance spectroscopy curves of P-LFP and R-LFP. (f) $z' \sim \omega^{-1/2}$ fitting curves for P-LFP and R-LFP. (g) The long-term cycling performance of P-LFP, D-LFP, and R-LFP at 1 C.

Regeneration of commercially degraded LFP cathodes harvested from spent prismatic cells

Based on the above experimental results, the external short-circuit relithiation method was applied to naturally degraded LFP cathodes from spent commercial prismatic cells to evaluate its practical application. Fig. S11 shows the optical images of the spent commercial prismatic cell before and after disassembling. The cathodes were cut into 12mm electrodes and then regenerated using this relithiation method. Fig. 5a shows the XRD pattern diffraction results of different lithiated materials. The typical diffraction $FePO_4$ peaks are at 18.10°, 30.44°, 30.98°, and 33.25° [31]. After relithiation, the typical diffraction peaks of $FePO_4$ in the commercial D-LFP disappeared. The XRD diffraction pattern of commercial R-LFP was contacted with the LFP standard diffraction peak (PDF #83–2902). Compared to lithium metal relithiation, the lithium graphite relithiation process is shorter and more efficient. Fig. S12 shows the FT-IR spectra of commercial D-LFP and R-LFP; the characteristic band of olivine $FePO_4$ at 1236.45 cm^{-1} can be clearly observed in the commercial D-LFP, which is not shown in the commercial R-LFP [47]. In the commercial D-LFP, the valence state of Fe and the lattice parameters had changed, leading to the change in the vibration frequency of the FT-IR spectrum. In the commercial R-LFP, the band of the symmetric stretching mode of PO_4^{3-} at 926.43 cm^{-1} had gradually shifted to 901.04 cm^{-1} [48,49]. The band at 631.13 cm^{-1} assigned to the octahedral FeO_6 vibration mode had shifted to 633.71 cm^{-1} [47,49]. Overall, the external short-circuit relithiation process did not disrupt the octahedral FeO_6 and tetrahedral PO_4 framework in the olivine structure, which is consistent with the results of the XRD analysis. Fig. 5b shows the Li-Fe ratio and initial charge capacity of commercial D-LFP and R-LFP cathodes; compared with commercial D-LFP, Li^+ was supplemented after relithiation in commercial R-LFP, and the initial charging capacity was restored.

SEM was used to explore the effects of the external short-circuit relithiation process on the morphology of commercial D-LFP and R-LFP cathodes (Fig. 5c). The CP and HRTEM images exhibit high similarity in the particle size for D-LFP and R-LFP, demonstrating no defects such as pores and microcracks in the internal structure. The microscopic details show that the lithium replenishment process did not damage the $LiFePO_4$ structure, which proved that the relithiation process has negligible effects on the morphology of the cathodes (Fig. S13). In the HRTEM image of D-LFP, the $FePO_4$ phase predominates, aligning with the XRD refinement results. The crystalline spacing measures 0.346 nm, corresponding to the (111) crystallite of $FePO_4$. Notably, some regions in D-LFP exhibit partial disorder (see Fig. S14). In the HRTEM image of R-LFP, the $FePO_4$ phase is transformed into $LiFePO_4$ phase with a crystal plane spacing of 0.518 nm, corresponding to the (200) crystal plane of $LiFePO_4$. Changes in cell size during the external short-circuit relithiation process were analyzed by Rietveld refinements performed on the commercial R-LFP and D-LFP cathodes with XRD and the different lithiated materials (Fig. 5d–f). The errors of XRD refinement results were less than 3%, ensuring the reliability of the results (Table S1). As the lithium embedding reaction proceeded, the cell size increased

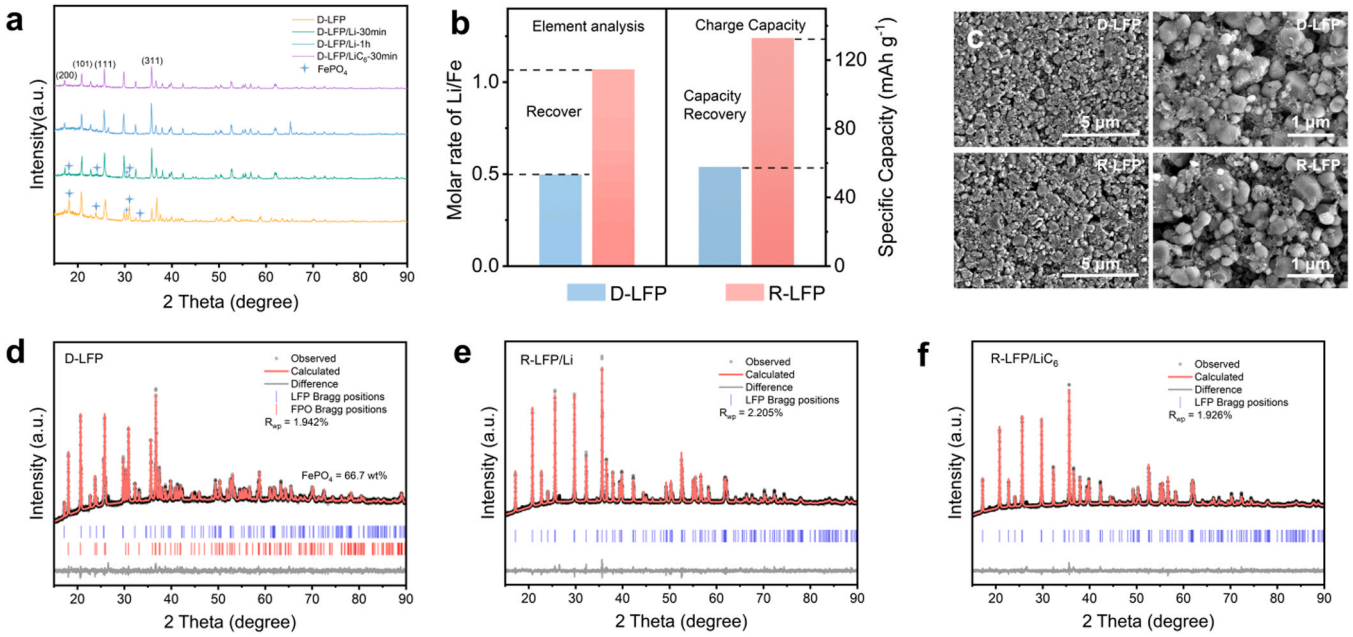


Fig. 5. The evaluation of potential applications for the external short-circuit relithiation method. (a) The XRD patterns of the commercial D-LFP and R-LFP with different lithiated materials. (b) The relative molar ratio of Li/Fe and the initial charge capacity of D-LFP and R-LFP at 0.1 C. (c) The SEM images for commercial D-LFP and R-LFP. The Rietveld refinement of the XRD pattern for (d) D-LFP and (e-f) R-LFP that was regenerated by Li and LiC_6.

significantly along the a and b axes while decreasing along the c axis [31]. This change in cell size is consistent with the characteristic transition from $FePO_4$ to $LiFePO_4$, indicating that lithium-ions were successfully inserted into olivine during the external short-circuit relithiation process [50,51].

Evaluation of the electrochemical performance of regenerated commercial LFP cathodes

The electrochemical performance of the commercial D-LFP and R-LFP cathodes was investigated with half coin cells from 2.5 to 4.0 V (Fig. 6a). The discharge capacity of the commercial D-LFP was 96.3 mAh g^{-1} after 70 cycles, and the discharge capacity of the commercial R-LFP was 121.6 mAh g^{-1} after 70 cycles. These results validate that the commercial R-LFP dramatically improved electrochemical performance after the relithiation process. Fig. 6b,c display the discharge capacities of the commercial R-LFP at varying currents were measured at 133.5 (0.1 C), 131.3 (0.2 C), 125.4 (0.5 C), 117.7 (1 C), and 99.1 mAh g^{-1} (2 C). When the charge-discharge current was restored to 0.5 C, the discharge capacity increased to 124.8 mAh g^{-1}, signifying that R-LFP cathodes maintained their original structure and electrochemical stability at higher discharge currents. Considering further applications for recycling, the full coin cells were assembled with the lithiated graphite from the disassembled prismatic cell as the counter electrode to compare the commercial R-LFP's electrochemical performance to the commercial D-LFP cathodes. For the R-LFP cathode, the initial charge capacity of commercial R-LFP was 118.5 mAh g^{-1} at 0.1 C. In contrast, the initial charge capacity of the commercial D-LFP was 58.8 mAh g^{-1} (Fig. 6d). Fig. 6e,f show the rate performance of full coin cells by using the discharge capacities under varying rates. The measurements were recorded as 134.7 (0.1 C), 131.9 (0.2 C), 125.5 (0.5 C), 116.8 (1 C), and 103.2 mAh g^{-1} (2 C). When the charge-discharge current was restored to 0.5 C, the discharge capacity increased to 121.1 mAh g^{-1}. This indicates that the commercial R-LFP full coin cell substantially improved electrochemical performance after relithiation. The commercial R-LFP full coin had superior electrochemical discharge capacity compared to the D-LFP full coin cell.

The long-term cycling stability of commercial D-LFP and R-LFP full coin cells at 0.5 C (Fig. 6g) was tested. The Li-deficiency commercial D-LFP degraded during the initial cycle. In contrast, the R-LFP showed discharge capacities of 125.1 mAh g^{-1} and 119.8 mAh g^{-1} after 300 cycles at 0.5 C with good capacity retention (98.8% after 100 cycles and 95.8% after 500 cycles), which was attributed to the supplementation of the lithium in commercial R-LFP. After long-term cycling, the full coin cell was disassembled to obtain the cycled LFP cathodes and graphite anodes. Fig. S15 and Fig. S16 show the SEM images of cycled LFP cathodes and graphite anodes, respectively. In comparing the surface morphology of LFP cathodes and graphite anodes before and after cycling, the LFP particles had smooth surfaces and complete structures. Still, the surfaces of the graphite anodes had cracks, and the original layer structure was damaged. These are the main reasons the battery capacity of LFPs degrades and eventually fails.

Economic and environmental analysis of different battery recycling technologies

Fig. 7a summarizes the pyramid model for maximizing the economic value of LIB recycling, where the direct cascade use of spent batteries is the recycling method for maximizing the monetary value of battery recycling. The second most economical value from recycling would come from the electrode material, with the most negligible value from individual battery elements. In this section, the EverBatt 2020 model developed by Argonne National Laboratory to estimate the total economic and environmental profit of four recycling technologies: pyro-recovery, hydro-recovery, direct materials, and electrode regeneration [52]. The model used one kilogram of spent LFP batteries and 0.457 kg of degraded LFP electrodes. This was based on the approximate proportion for each spent battery component. The model representing spent LFP is $Li_{0.8}FePO_4$, which determines the cost and revenue of different recycling routes. For the hydro route, a standard sulfuric acid leaching technology was selected as the reference [53]. Fig. 7b displays the cost of different routes based on market prices in China. Consumption of raw materials is the main cost in recycling spent batteries, accounting for ~74.5% of the total cost in the pyro-recovery route and ~49.5% in the hydro-recovery route (Fig. S17 and Table S2). In comparison, lithium salts are an important contributor to the total cost in the direct materials

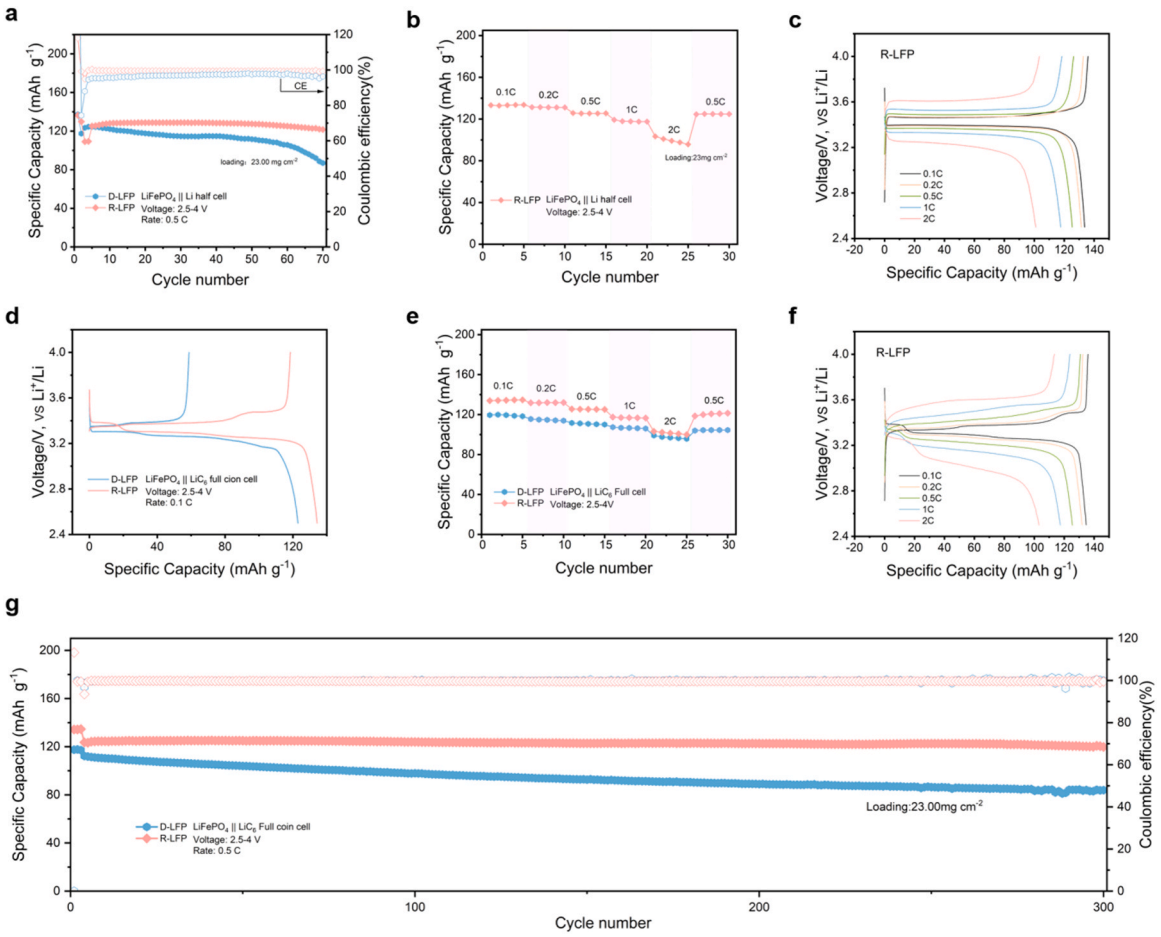


Fig. 6. The electrochemical performance of regenerated commercial LFP cathodes. (a) The cycle performance of commercial D-LFP and R-LFP half coin cells. (b) The rate performance of commercial D-LFP and R-LFP half coin cells. (c) The charge and discharge profiles of commercial R-LFP in different rates. (d)The initial charge and discharge profiles of commercial D-LFP and R-LFP full coin cells. (e) The rate performance of commercial D-LFP and R-LFP full coin cells. (f) The charge and discharge profiles of commercial R-LFP in different rates of full coin cells (g) The long-term cycling performance of commercial D-LFP and R-LFP full coin cells at 0.5 C.

route.

Profitability will be a key factor in the emergence of a sustainable and circular LIBs recycling industry [5,21]. Lithium carbonate and iron phosphate are the main revenue in the hydro route (Fig. 7c). Due to the low residual lithium in degraded LFP batteries, lithium carbonate production in the final product is lower. For the direct routes, the LFP materials after regeneration are the main components in revenue, with a percentage of ~64.5%. In contrast, the LFP-regenerated electrodes account for about 70.6% (Fig. S18 and Table S3). The direct electrode route can recover separators and battery shells, slightly improving revenue. The profit produced by the hydro route is \$3.00 kg^{-1} per cell, and the direct materials route is 4.69 kg^{-1} per cell. Whereas the profits produced by the direct electrode regeneration is \$6.24 kg^{-1} per cell (Fig. S19 and Table S4). The direct electrode regeneration route is the most profitable of all available methods.

Energy consumption and greenhouse gas (GHG) emissions are important considerations for developing a sustainable recycling system. The total energy consumption of the pyro and hydro processes is 12.14 and 19.57 MJ kg^{-1} per cell (Fig. 7d). In hydroprocessing, 89.2% of energy consumption comes from the acid leaching, metal extraction, and precipitation steps. In contrast, the energy consumption process of the direct materials route requires 16.75 MJ kg^{-1} per cell from the heat treatment during regeneration. The direct electrode regeneration route only requires 6.29 MJ kg^{-1} per cell. The total GHG emissions for pyro, hydro, and direct materials route processes are 1.96, 1.49, and 1.83 kg^{-1} per cell, respectively. The total GHG emission from the direct electrode route was 0.56 kg kg^{-1} per cell (Fig. 7e). The results above indicate that direct electrode regeneration reduces material consumption, simplifies operation procedures, and improves environmental protection and energy conservation. Four battery recycling technologies were compared, andthe conclusions are summarized in Fig. 7f. The direct electrode route has two advantages: electrodes are valuable, and the process is straightforward [54]. Therefore, the direct electrode regeneration route holds promise for the future recycling industry.

Conclusion

This research proposes an efficient and direct relithiation method to regenerate the degraded $LiFePO_4$ cathode using an external short-circuit process at room temperature. Utilizing a discharge process to form an external short-circuit structure by combining lithiated materials with Li-deficient $Li_{1-x}FePO_4$, the created potential serves as the driving force to supplement lithium ions into the lithium vacancies of the $Li_{1-x}FePO_4$ material. Using Li-deficiency cathodes obtained by disassembling spent LFP prismatic cells greatly simplifies the pre-processing and recycling costs by reducing energy, reagent, and fixed facility cost. The artificially degraded $Li_{1-x}FePO_4$ and the degraded LFP obtained from the spent commercial prismatic cells were revived through controlling time for the relithiation process. The renewed LFP cathode demonstrates comparable long-term stability and superior rate capacity over the degraded LFP cathode. Few studies have investigated the direct regeneration of cathode material, and the relithiation strategy presented in this work

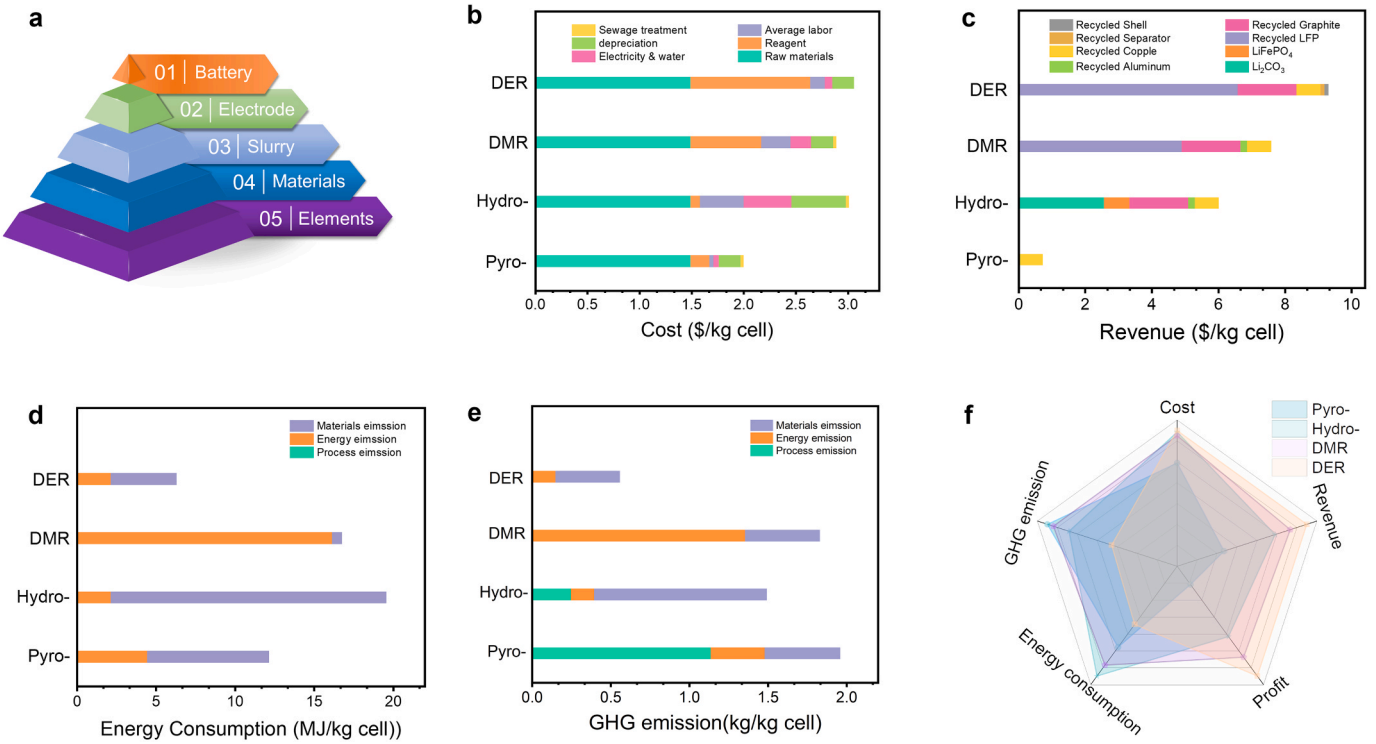


Fig. 7. The economic and environmental analysis of different battery recycling processes. (a) The current pyramid model for maximizing the monetary value of LIB recycling. (b) The cost and (c) revenue splits based on the pyro, hydro, direct material, and electrode regeneration routes. (d) Total energy consumption and (e) GHG emissions of recycling 1 kg spent LFP batteries based on the pyro, hydro, direct material, and electrode regeneration routes. (f) Comprehensive comparison of battery recycling technologies.

demonstrates a unique approach to regenerating the spent cathodes from LIBs. Reviewing LIB recycling from a regeneration perspective offers LIB recyclers a significant opportunity to improve next-generation methods with practical applications.

Experimental section

Materials

Battery grade lithium metal foil was purchased from China Energy Lithium Co., Ltd. N-methyl-2-pyrrolidone (NMP) was purchased from Shanghai Aladdin Bio-Chem Technology Co., Ltd. $LiPF_6$ (1 M) in ethylene carbonate (EC): dimethyl carbonate (DMC): ethyl methyl carbonate (EMC) (1:1:1 vol%) was purchased from Suzhou Dodo Chemical Technology Co., Ltd. LFP materials were purchased from Shenzhen Dynanonic Co., Ltd. Spent commercial LFP batteries, battery grade Super P, and PVDF binder were purchased from Guangdong Canrd New Energy Technology Co., Ltd.

The preparation of delithiated $Li_{1-x}FePO_4$ cathodes

The LFP cathodes were prepared using a slurry created by mixing LFP powder, Super-P, and PVDF at an 8:1:1 ratio by mass. The cathodes were assembled into coin cells, and the cell's charge time was controlled at a charge current of 0.1 C to obtain cathodes with different Li-deficiencies. The charged coin cell was disassembled in the glove box, cleaned with dimethyl carbonate, and dried in a vacuum oven for four hours to obtain $Li_{1-x}FePO_4$ cathodes with various Li-deficiencies.

The preparation of spent Prismatic LFP cell cathodes

Spent commercial LFP prismatic cells were discharged to 2.5 V, transferred into a glove box, manually disassembled, and washed with dimethyl carbonate to remove lithium salt residues. The cathodes were dried in a vacuum oven for four hours to procure the commercial Li-deficiency cathodes.

The regeneration of LFP cathodes through an external short-circuit method

The Li-deficiency $Li_{1-x}FePO_4$ cathodes were transferred into the glovebox (under an argon atmosphere), and aluminum foils were used as the external conductors. The lithiated material was put on the aluminum foil with an appropriate amount of electrolyte, and the polypropylene separators (PP) were positioned onto the lithiated material. The $Li_{1-x}FePO_4$ cathodes were placed on the PP separators and wrapped with aluminum foil. The reaction time was used to control the regeneration process. After the reaction, the cathodes were cleaned with dimethyl carbonate and dried in a vacuum oven for four hours to obtain the regenerated LFP cathodes.

Characterization of the degraded and regenerated LFP cathodes

Field emission scanning electron microscope (FESEM, SU-8010, Hitachi) and high-resolution transmission electron microscopy (HRTEM, Tecnai G2 F30, FEI) were conducted to assess the morphology and microstructure of the materials. X-ray diffraction spectroscopy (XRD, D8 Advance, Bruker) was used to characterize the crystal structures of the pristine LFP, degraded LFP, and regenerated LFP. Inductively coupled plasma spectrometry (ICP, Arcos II MV, SPECTRO) was used to determine the elemental contents of the degraded LFPs and regenerated LFPs. X-ray photoelectron spectroscopy (XRS, 5000 V VersaProbeII, ULVCA-PHI) was used to analyze the elemental valence on the LFP cathode surface. The cathodes were cut with an ion beam thinning device (RES102, LEICA) and a triple ion beam cutting and polishing device (CP, M1061, FISCHIONE). Electrochemical properties were evaluated using the LAND battery test system (Wuhan Land,

CT2001A, China). A test that uses a half coin cell (CR 2032) and lithium foil as the counter electrode, with a potential range of 2.5–4.0 V at 0.1 C (1 C=135 mAh g^{-1}). Cycling and rate performance tests at various current densities were performed with a 2.5–4.0 V potential range. Electrochemical impedance spectroscopy and cyclic voltammetry (EIS/CV, BioLogic Science Instruments, France) were measured using a VMP3 multichannel electrochemical workstation.

Economic and environmental analysis of different battery recycling technologies

To demonstrate the savings and benefits of our proposed methodology compared to other main stream ones, we have performed a thorough economic and environmental analysis, with the primary focus of the economic analysis is D-LFP recycling for one kilogram of cathode material. The financial cost was divided into six parts: raw materials, reagents, average labor, water and electricity, equipment depreciation, and sewage treatment. The values of the separators, electrolytes, and battery shells were challenging to assess in the pyro recovery, hydro recovery, and direct material regeneration processes, so these components were omitted in the revenue analysis. The values of the separator and battery shells were evaluated for the direct electrode regeneration process. The $Li_{0.8}FePO_4$ model was used as a baseline for assessing the D-LFP cathode recycling. The detailed process-based costs, revenues, and profits are shown in the original data of the techno-economic analysis (Tables S7-S15).

Based on the EverBatt 2020 model developed by Argonne National Laboratory, a complete life cycle and techno-economic analysis of pyro recovery, hydro recovery, direct material, and electrode regeneration processes were performed. The material requirements for pyro recovery, hydro recovery, and direct material regeneration were derived from the EverBatt 2020 model. This work's results were used to calculate the direct regeneration of cathodes. The four recycling processes' total energy consumption and emissions comprised of material, energy, and process emissions showed in Tables S5–S6.

Declaration of Competing Interest

The authors declare that they have no known competing financial interests or personal relationships that could have appeared to influence the work reported in this paper.

Acknowledgments

This research was financially supported by the Research and Application Demonstration of Physical Discharge Media for Spent Lithium-Ion Batteries (No. 202210213000003), National Natural Science Foundation of China (No. 52261160384 and 52072208), Fundamental Research Project of Shenzhen (No. JCYJ20220818101004009), Local Innovative and Research Teams Project of Guangdong Pearl River Talents Program (2017BT01N111), Sheen Science and Technology Program (KCXFZ20211020163810015), Guangdong Basic and Applied Basic Research Foundation (No. 2022A1515110531), and China Postdoctoral Science Foundation (No. 2022M721800). We also acknowledge the support of the Testing Technology Center of Materials and Devices of Tsinghua Shenzhen International Graduate School (SIGS), and the Major Science and Technology Infrastructure Project of Material Genome Bigscience Facilities Platform supported by Municipal Development and Reform Commission of Shenzhen. Bo Lan would like to acknowledge support from the Imperial College Research Fellowship scheme.

Appendix A. Supporting information

Supplementary data associated with this article can be found in the online version at doi:10.1016/j.nxsust.2023.100008.

References

[1] X. Zhao, C.D. Otto, E.T. Wallace, et al., The economic competitiveness and emissions of battery electric vehicles in China, Appl. Energy 156 (2015) 666–675.
[2] Y. Zhao, Y. Kang, J. Wozny, et al., Recycling of sodium-ion batteries, Nat. Rev. Mater. 8 (2023) 623–634.
[3] J. Mao, C. Ye, S. Zhang, et al., Toward practical lithium-ion battery recycling: adding value tackling circularity and recycling-oriented design, Energy Environ. Sci. 15 (2022) 2732–2752.
[4] C. Wu, J. Hu, L. Ye, et al., Direct regeneration of spent Li-ion battery cathodes via chemical relithiation reaction, ACS Sustain. Chem. Eng. 9 (2021) 16384–16393.
[5] Y. Yue, G. Emenike, Y.H. Guo, et al., On the sustainability of lithium ion battery industry-A review and perspective, Energy Storage Mater. 36 (2021) 186–212.
[6] J. Wang, Z. Liang, Y. Zhao, et al., Direct conversion of degraded $LiCoO_2$ cathode materials into high-performance $LiCoO_2$: a closed-loop green recycling strategy for spent lithium-ion batteries, Energy Storage Mater. 45 (2022) 768–776.
[7] Y. Kang, Z. Liang, Y. Zhao, et al., Large-scale synthesis of lithium-and manganese-rich materials with uniform thin-film Al_2O_3 coating for stable cathode cycling, Sci. China Mater. 63 (2020) 1683–1692.
[8] M.M. Thackeray, K. Amine, $LiMn_2O_4$ spinel and substituted cathodes, Nat. Energy 6 (5) (2021), 566-566.
[9] M.C. Fan, Y. Zhao, Y.Q. Kang, et al., Room-temperature extraction of individual elements from charged spent $LiFePO_4$ batteries, Rare Met. 41 (5) (2022) 1595–1604.
[10] H. Gavin, S. Roberto, K. Emma, et al., Recycling lithium-ion batteries from electric vehicles, Nature 575 (2019) 75–86.
[11] F. Ersha, L. Li, W. Zhenpo, et al., Sustainable recycling technology for Li-ion batteries and beyond, Challenges and future prospects, Chem. Rev. 120 (2020) 7020–7063.
[12] H. Wang, S. Zhang, B. Li, et al., Recovery of waste printed circuit boards through pyrometallurgical processing a review, Resour. Conserv. Recycl. 126 (2017) 209–218.
[13] Y. Zhao, Y. Kang, M. Fan, et al., Precise separation of spent lithium-ion cells in water without discharging for recycling, Energy Storage Mater. 45 (2022) 1092–1099.
[14] P.F. Xiao, H.S. Chun, F.L. Xi, et al., Separation and recovery of valuable metals from spent lithium-ion batteries via concentrated sulfuric acid leaching and regeneration of $LiNi_{1/3}Co_{1/3}Mn_{1/3}O_2$, J. Alloy. Compd. 863 (2021), 158775.
[15] Y. Song, B. Xie, S. Song, et al., Regeneration of $LiFePO_4$ from spent lithium-ion batteries via a facile process featuring acid leaching and hydrothermal synthesis, Green. Chem. 23 (11) (2021) 3963–3971.
[16] Y. Li, W. Lv, H. Huang, et al., Recycling of spent lithium-ion batteries in view of green chemistry, Green. Chem. 23 (17) (2021) 6139–6171.
[17] L. Zhang, Z. Xu, Z. He, Electrochemical relithiation for direct regeneration of $LiCoO_2$ materials from spent lithium-ion battery electrodes, ACS Sustain. Chem. Eng. 8 (2020) 11596–11605.
[18] H. Du, Y. Kang, C. Li, et al., Easily recyclable lithium-ion batteries Recycling-oriented cathode design using highly soluble $LiFeMnPO_4$ with a water-soluble binder, Battery Energy 2 (2023) 20230011.
[19] K. Peng, L. Zhang, Sustainable recycling of electrode materials in spent Li-ion batteries through direct regeneration processes, ACS EST Eng. 2 (2022) 586–605.
[20] Q. Jing, J. Zhang, Y. Liu, et al., Direct regeneration of spent $LiFePO_4$ cathode material by a green and efficient one-step hydrothermal method, ACS Sustain. Chem. Eng. 8 (48) (2020) 17622–17628.
[21] P. Xu, Q. Dai, H. Gao, et al., Efficient direct recycling of lithium-ion battery cathodes by targeted healing, Joule 4 (12) (2020) 2609–2626.
[22] J. Ma, J. Wang, K. Jia, et al., Adaptable eutectic salt for the direct recycling of highly degraded layer cathodes, J. Am. Chem. Soc. 144 (44) (2022) 20306–20314.
[23] Y. Shi, M. Zhang, Y.S. Meng, et al., Ambient-pressure relithiation of degraded $LixNi_{0.5}Co_{0.2}Mn_{0.3}O_2$ ($0< x< 1$) via eutectic solutions for direct regeneration of lithium-ion battery cathodes, Adv. Energy Mater. 9 (20) (2019) 1900454.
[24] D. Peng, X. Wang, S. Wang, et al., Efficient regeneration of retired $LiFePO_4$ cathode by combining spontaneous and electrically driven processes, Green. Chem. 24 (11) (2022) 4544–4556.
[25] Z. Jiang, J. Sun, P. Jia, et al., A sustainable strategy for spent Li-ion battery regeneration: microwave-hydrothermal relithiation complemented with anode-revived graphene to construct a $LiFePO_4$/MWrGO cathode material, Sustain. Energy Fuels 6 (9) (2022) 2207–2222.
[26] X. Zhang, Q. Xue, L. Li, et al., Sustainable recycling and regeneration of cathode scraps from industrial production of lithium-ion batteries, ACS Sustain. Chem. Eng. 4 (12) (2016) 7041–7049.
[27] F. Zheng, L.D. Qiang, K.P. Qing, et al., Comparative study of chemical discharge strategy to pretreat spent lithium-ion batteries for safe efficient and environmentally friendly recycling, J. Clean. Prod. 359 (2022), 132116.
[28] L. Yang, K. Yang, J. Zheng, et al., Harnessing the surface structure to enable high-performance cathode materials for lithium-ion batteries, Chem. Soc. Rev. 49 (14) (2020) 4667–4680.
[29] X. Liu, Y.J. Wang, B. Barbiellini, et al., Why $LiFePO_4$ is a safe battery electrode: coulomb repulsion induced electron-state reshuffling upon lithiation, Phys. Chem. Chem. Phys. 17 (39) (2015) 26369–26377.
[30] T. Wang, X. Yu, M. Fan, et al., Direct regeneration of spent $LiFePO_4$ via a graphite prelithiation strategy, Chem. Commun. 56 (2) (2020) 245–248.
[31] J.H. Kim, S.C. Woo, M.S. Park, et al., Capacity fading mechanism of $LiFePO_4$-based lithium secondary batteries for stationary energy storage, J. Power Sources 229 (2013) 190–197.

[32] N. Paul, J. Wandt, S. Seidlmayer, et al., Aging behavior of lithium iron phosphate based 18650-type cells studied by in situ neutron diffraction, J. Power Sources 345 (2017) 85–96.
[33] Y.Z. Dong, Y.M. Zhao, H. Duan, Crystal structure and lithium electrochemical extraction properties of olivine type $LiFePO_4$, Mater. Chem. Phys. 129 (3) (2011) 756–760.
[34] A.K. Padhi, K.S. Nanjundaswamy, J.B. Goodenough, Phospho-olivines as positive-electrode materials for rechargeable lithium batteries, J. Electrochem. Soc. 144 (4) (1997) 1188.
[35] M. Takahashi, S. Tobishima, K. Takei, et al., Characterization of $LiFePO_4$ as the cathode material for rechargeable lithium batteries, J. Power Sources 97 (2001) 508–511.
[36] C. Wu, M. Xu, C. Zhang, et al., Cost-effective recycling of spent $LiMn_2O_4$ cathode via a chemical lithiation strategy, Energy Storage Mater. 55 (2023) 154–165.
[37] Y. Kobayashi, H. Miyashiro, A. Yamazaki, et al., Unexpected capacity fade and recovery mechanism of $LiFePO_4$/graphite cells for grid operation, J. Power Sources 449 (2020), 227502.
[38] G. Ji, J. Wang, Z. Liang, et al., Direct regeneration of degraded lithium-ion battery cathodes with a multifunctional organic lithium salt, Nat. Commun. 14 (1) (2023) 584.
[39] M. Fan, Q. Meng, X. Chang, et al., In situ electrochemical regeneration of degraded $LiFePO_4$ electrode with functionalized prelithiation separator, Adv. Energy Mater. 12 (18) (2022) 2103630.
[40] M. Fan, X. Chang, X.H. Meng, et al., Structural restoration of degraded $LiFePO_4$ cathode with enhanced kinetics using residual lithium in spent graphite anodes, CCS Chem. 5 (2022) 1189–1201.
[41] M.Y. Li, F.F. Yu, Q.W. Chao, et al., Closed-loop regeneration of battery-grade $FePO_4$ from lithium extraction slag of spent Li-ion batteries via phosphoric acid mixture selective leaching, Chem. Eng. J. 431 (2022), 133232.
[42] X.H. Yue, C.C. Zhang, W.B. Zhang, et al., Recycling phosphorus from spent $LiFePO_4$ battery for multifunctional slow-release fertilizer preparation and simultaneous recovery of Lithium, Chem. Eng. J. 426 (2021), 131311.
[43] M. Hess, T. Sasaki, C. Villevieille, et al., Combined operando X-ray diffraction–electrochemical impedance spectroscopy detecting solid solution reactions of $LiFePO_4$ in batteries, Nat. Commun. 6 (1) (2015) 8169.
[44] J. Yang, W. Wang, H. Yang, et al., One-pot compositional and structural regeneration of degraded $LiCoO_2$ for directly reusing it as a high-performance lithium-ion battery cathode, Green. Chem. 22 (19) (2020) 6489–6496.
[45] Y. Ma, X. Zhou, J. Tang, et al., One-step selective recovery and cyclic utilization of valuable metals from spent lithium-ion batteries via low-temperature chlorination pyrolysis, Resour. Conserv. Recycl. 175 (2021), 105840.
[46] G. Liang, Z. Wu, C. Didier, et al., A long cycle-life high-voltage spinel lithium-ion battery electrode achieved by site-selective doping, Angew. Chem. Int. Ed. 132 (26) (2020) 10681–10689.
[47] A.A. Salah, P. Jozwiak, K. Zaghib, et al., FTIR features of lithium-iron phosphates as electrode materials for rechargeable lithium batteries, Spectrochim. Acta Part A: Mol. Biomol. Spectrosc. 65 (5) (2006) 1007–1013.
[48] C.M. Burba, R. Frech, Raman and FTIR spectroscopic study of Li_xFePO_4 ($0 \leq x \leq 1$), J. Electrochem. Soc. 151 (7) (2004) A1032.
[49] P. Jozwiak, J.E. Garbarczyk, M. Wasiucionek, et al., DTA, FTIR and impedance spectroscopy studies on lithium–iron–phosphate glasses with olivine-like local structure, Solid State Ion. 179 (1–6) (2008) 46–50.
[50] J. Ni, Y. Zhao, J. Chen, et al., Site-dependent electrochemical performance of Mg doped $LiFePO_4$, Electrochem. Commun. 44 (2014) 4–7.
[51] P. Gibot, M. Casas-Cabanas, L. Laffont, et al., Room-temperature single-phase Li insertion/extraction in nanoscale Li_xFePO_4, Nat. Mater. 7 (9) (2008) 741–747.
[52] Dai Q., Gaines L., Spangenberger J., et al. Everbatt: A closed-loop battery recycling cost and environmental impacts model (2019) ⟨www.Anl.Gov/egs/everbatt⟩.
[53] H. Li, S. Xing, Y. Liu, et al., Recovery of lithium, iron, and phosphorus from spent $LiFePO_4$ batteries using stoichiometric sulfuric acid leaching system, ACS Sustain. Chem. Eng. 5 (9) (2017) 8017–8024.
[54] J. Piątek, S. Afyon, T.M. Budnyak, et al., Sustainable Li-ion batteries: chemistry and recycling, Adv. Energy Mater. 11 (43) (2021) 2003456.